Comparison of Small Molecule and Polymeric Urethanes, Thiourethanes, and Dithiourethanes: Hydrogen Bonding and Thermal, Physical, and Mechanical Properties

Qin Li,[†] Hui Zhou,[†] Douglas A. Wicks,[†] Charles E. Hoyle,*[,†] David H. Magers,[‡] and Harley R. McAlexander[‡]

School of Polymers and High Performance Materials, University of Southern Mississippi, Hattiesburg, Mississippi 39401, and Department of Chemistry and Biochemistry, Mississippi College, Clinton, Mississippi 39056

Received December 23, 2008; Revised Manuscript Received January 8, 2009

ABSTRACT: The hydrogen bonding behavior of a homologous series of small molecule and polymeric urethanes, thiourethanes, and dithiourethanes was investigated in solution, melt, and solid states. The relative hydrogen bonding strengths in both small molecule and polymer systems were evaluated, and the results were compared to theoretical calculations of hydrogen bonding strength. The results for NMR and FTIR analysis of the small molecule models indicated that the NH protons on the carbamate and thiocarbamates have greater hydrogen bonding strengths than the NH protons of the dithiocarbamate. The polyurethane and polythiourethanes were found to have approximately equivalent physical and mechanical properties as a result of a similar extent of hydrogen bonding, whereas the polydithiourethane, due to a lower degree of hydrogen bonding, has reduced thermal and mechanical transition temperatures as well as lower hardness values. The polythiourethane and polydithiourethane networks exhibit narrower glass transitions compared to polyurethane networks, apparently the result of an efficient isocyanate/isothiocyanate−thiol reaction with little or no side products. Because of weakness of the C−S bond compared to the C−O bond, thiourethanes and dithiourethanes have lower thermal stability than the corresponding urethanes. Finally, the polythiourethanes and polydithiourethane have higher refractive index values than their polyurethane counterpart.

Introduction

Polyurethanes, since their discovery in the 1930s and first report in 1947,[1] have been widely used in many coatings[2] and elastomer[3] applications due to an extraordinary combination of physical and mechanical properties. Accordingly, the structure−property relationships of polyurethanes have been extensively studied.[2,4−11] Hydrogen bonding, providing physical linkages within the material matrix, is a vital factor that determines the microscopic and macroscopic properties of polyurethanes, including their phase behavior, glass transition temperature, strength, and stiffness.[8,9] Considerable effort has been extended to understand the hydrogen bonding behavior of polyurethanes in both segmented systems and polymer blends.[4,6,10,11]

Although the reactions of thiols and isocyanates have also been known for a long time[12,13] and the resultant polythiourethanes (containing a structure unit as −N(H)−C(═O)−S−) are used in many modern applications including optical lenses due to high refractive index values[14,15] and advanced coatings,[16−18] the basic physical and mechanical properties of the polythiourethanes have not been characterized to the same extent as polyurethane counterparts, although limited literature can be found on their synthesis/catalysis,[12,13] reaction kinetics,[19] thermodynamic transitions,[20] and hydrogen bonding.[21,22] Also, the physical properties of polymers based on a similar dithiourethane unit, −N(H)−C(═S)−S−, and explored for use in optical applications due to their high refractive index values,[14,15] have not been extensively evaluated.

One of the distinct advantages of the thiourethane and dithiourethane chemical structural units is the feasibility of incorporating them into photopolymerizable systems which has the potential of opening up whole new application areas. For example, in our previous study on photopolymerized thiol−ene films,[23] a notable enhancement in glass transition temperature was attained for thiourethane−thiol−ene (TUTE) systems presumably due to several factors including the hydrogen bonding associated with the thiourethane linkages. However, questions related to the strength of the hydrogen bonds of polythiourethanes and polydithiourethanes compared with those of ordinary polyurethanes and the corresponding effect on polymer properties remain to be delineated.

From both a basic and practical viewpoint, a detailed investigation and comparative analysis of the hydrogen bonding behavior of a homologous family of structures including urethanes (−N(H)−C(═O)−O−), thiourethanes (−N(H)−C(═O)−S−), and dithiourethanes (−N(H)−C(═S)−S−), and the resulting correlation of polymer structure and physical, mechanical, and optical properties is important in establishing guidelines for future development. Accordingly, to provide a comprehensive understanding of the hydrogen bonding behavior of each urethane type (polyurethane, polythiourethane, and polydithiourethane) and to characterize critical structure−property relationships, a series of small molecule carbamate model compounds were synthesized. The relative strength of their hydrogen bonds was measured in solution and melt, and the results were correlated with theoretical calculations. On the basis of the results of these simplified carbamate model systems, a contiguous set of polyurethane, polythiourethane, and polydithiourethane networks were evaluated, and the effect of hydrogen bonding on physical and mechanical properties was determined. The polyurethane and polythiourethanes were found to exhibit similar properties, quite different from those of polydithiourethanes, apparently due to differences in hydrogen bonding. The results reported herein are important in providing a clear theoretical and experimental basis for tailoring polymer proper-

* To whom correspondence should be addressed. E-mail: charles.hoyle@usm.edu.
[†] University of Southern Mississippi.
[‡] Mississippi College.

10.1021/ma802848t CCC: $40.75
Published on Web 02/27/2009

Scheme 1. Synthesis of Carbamate (HIHA), Thiocarbamates (HIHT and BMPHI), and Dithiocarbamate (BMPHIT)

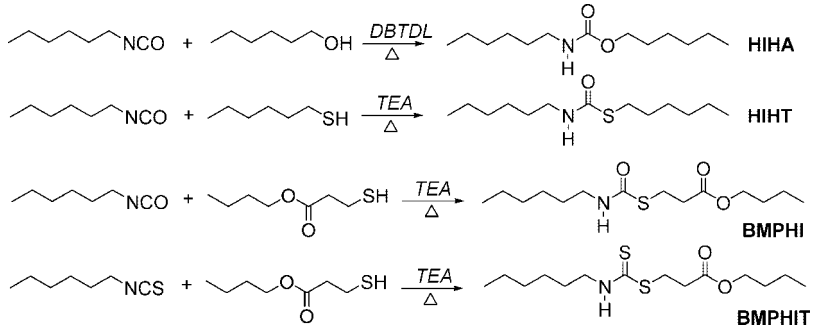

ties through introducing different urethane type linkages, i.e., urethanes, thiourethanes, and dithiourethanes.

Experimental Section

Materials. Chemicals for model compound synthesis, hexyl isocyanate (HI), hexyl isothiocyanate (HIT), 1-hexanol (HA), 1-hexanethiol (HT), butyl 3-mercaptopropionate (BMP), 1,6-hexanediol (HexDiol), 1,6-hexanedithiol (HexDithiol), dibutyltin dilaurate (DBTDL), and triethylamine (TEA), were purchased from Aldrich Chemical Co. and used as received. 1,6-Hexamethylene diisocyanate (HDI) and the HDI trimer or Desmodur N3600 (3NCO) were obtained from Bayer Materials Science and used as received. 1,6-Hexane diisothiocyanate (HDIT) was purchased from Trans World Chemicals Inc. and used as received. Trimethylolpropane tris(3-mercaptopropionate) (TriThiol) was obtained from Bruno Bock Thiochemical and used as received. Other chemicals, such as anhydrous acetone, were also obtained from Aldrich Chemical Co. and used as received.

Preparation. Typical procedures for synthesizing the small molecule model compounds listed in Scheme 1, *N*-hexyl hexylcarbamate (HIHA), *N*-hexyl *S*-hexylcarbamate (HIHT), and *N*-hexyl *S*-butyl-3-mercaptopropionate thiocarbamate (BMPHI), and *N*-hexyl *S*-butyl-3-mercaptopropionate dithiocarbamate (BMPHIT), are as follows (HIHA is taken as an example). 0.03 mol of hexyl isocyanate and 0.03 mol of 1-hexanol were first charged into a three-neck flask before 10 mL of hexane was added. The reactor was then purged with dry N_2 for 30 min followed by 0.02 wt % of dibutyltin dilaurate (DBTDL) being added and stirred. The mixture was allowed to react for 8 h at 65 °C under dry N_2 flow. All the model products were purified by recrystallization from hexane 2−3 times, and their structures were verified by nuclear magnetic resonance spectroscopy (NMR). TEA was used as a catalyst in all thiol reactions with isocyanates or isothiocyanates due to its high efficiency.[24] DBTDL was used in all alcohol reactions.

^{1}H NMR. HIHA ($CDCl_3$): δ 0.89 (t, 6H, $-CH_3$), 1.30 (m, 12H, $-CH_2-$), 1.55 (m, 4H, $-CH_2-$), 3.17 (q, 2H, $-CH_2-$N), 4.04 (t, 2H, $-CH_2-$O−), 4.60 (s, 1H, −N(H)−).

HIHT ($CDCl_3$): δ 0.88 (t, 6H, $-CH_3$), 1.29 (m, 12H, $-CH_2-$), 1.55 (m, 4H, $-CH_2-$), 2.90 (q, 2H, $-CH_2-$N), 3.29 (t, 2H, $-CH_2-$S−), 5.25 (s, 1H, −N(H)−).

BMPHI ($CDCl_3$): δ 0.93 (t, 6H, $-CH_3$), 1.29 (m, 8H, $-CH_2-$), 1.56 (m, 4H, $-CH_2-$), 2.69 (t, 2H, $-CH_2-C(=O)-$), 3.15 (t, 2H, $-CH_2-$S−), 3.27 (q, 2H, $-CH_2-$N), 4.10 (t, 2H, $-CH_2-$O−), 5.27 (s, 1H, −N(H)−).

BMPHIT ($CDCl_3$): δ 0.93 (t, 6H, $-CH_3$), 1.32 (m, 8H, $-CH_2-$), 1.56 (m, 4H, $-CH_2-$), 2.77 (t, 2H, $-CH_2-C(=S)-$), 3.51 (t, 2H, $-CH_2-$S−), 3.72 (q, 2H, $-CH_2-$N), 4.11 (t, 2H, $-CH_2-$O−), 7.02 (s, 1H, −N(H)−).

To prepare the polymeric networks, 3NCO-HexDiol and 3NCO-HexDithiol (Scheme 2), 0.02 mol of 3NCO and 0.03 mol of HexDiol (or HexDithiol) were first charged into a scintillation vial before 2 mL of anhydrous acetone was added to form a transparent solution. ∼0.03 wt % (based on the whole mixture) of DBTDL (or ∼0.003 wt % of TEA) was then added to the monomer solution and mixed homogeneously. The solution was then evenly coated

Scheme 2. Preparation of Polyurethane (3NCO-HexDiol), Polythiourethanes (3NCO-HexDithiol and HDI-TriThiol), and Polydithiourethane (HDIT-TriThiol)

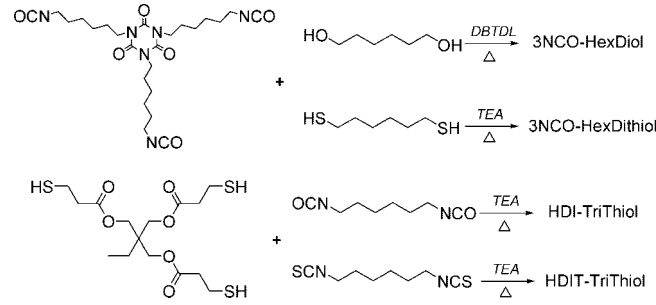

onto a piece of clean glass, followed by purging with dry N_2 in a sealable chamber for 1 h at room temperature, curing at 80 °C overnight and heating under vacuum (70 °C) for about 24 h. This yielded completely cured 200 μm thick films with no trace of solvent (verified by FTIR at 2272 cm^{-1} and thermal gravimetric analysis). To prepare HDI-TriThiol and HDIT-TriThiol (Scheme 2), 0.006 mol of TriThiol and 0.009 mol of HDI (or HDIT) were charged into a scintillation vial and mixed homogeneously before 0.01 wt % (or 0.4 wt %) of TEA was added. The mixture was then coated onto a piece of clean glass using a 5 mil draw down bar, followed by purging with dry N_2 in a sealable chamber for 1 h, curing at 80 °C overnight and then heating under vacuum to yield transparent films with thicknesses of ∼120 μm. The HDI-TriThiol films were completely cured (total loss of NCO groups at ∼2272 cm^{-1}), and the conversion of isothiocyanate groups (∼2082 cm^{-1}) in HDIT-TriThiol films was ∼99%. The type and concentration of catalysts were adjusted for each system, as described above, to achieve efficient curing, while also allowing enough time for mixing and film coating.

Characterization. Proton nuclear magnetic resonance (^{1}H NMR) spectra were obtained on a Mercury 300 (Varian Inc.) spectrometer, the temperature of which was controlled by a Bruker variable temperature unit equipped with a Eurotherm 818 controller. Each spectrum was recorded as the co-addition of 64 scans after 25 min of equilibrium at the desired temperature. For regular NMR measurements, concentrations of 3.7 mM (in either $CDCl_3$ or d-DMSO) were used for small molecules in solution. Regular and temperature-resolved infrared spectra were collected on a Bruker IFS 88 FTIR spectrometer by holding samples (small molecules or polymer films prepared) sandwiched between two NaCl plates in a heating unit controlled by a Harrick temperature controller with an accuracy of ±1 °C. Each spectrum was recorded after equilibrating for 25 min at the desired temperature. Peak deconvolution was conducted using a Gaussian function in Origin software to obtain free and hydrogen bonded NH peaks as described elsewhere.[25] Thermal stability of model polymers were measured with a TA Q60 (TA Instruments, Inc.) thermal gravimetric analysis (TGA) instrument operating at a heating rate of 20 °C/min in a N_2 atmosphere. Glass transition temperatures were measured with a TA Q1000 differential scanning calorimetry (DSC) operating at

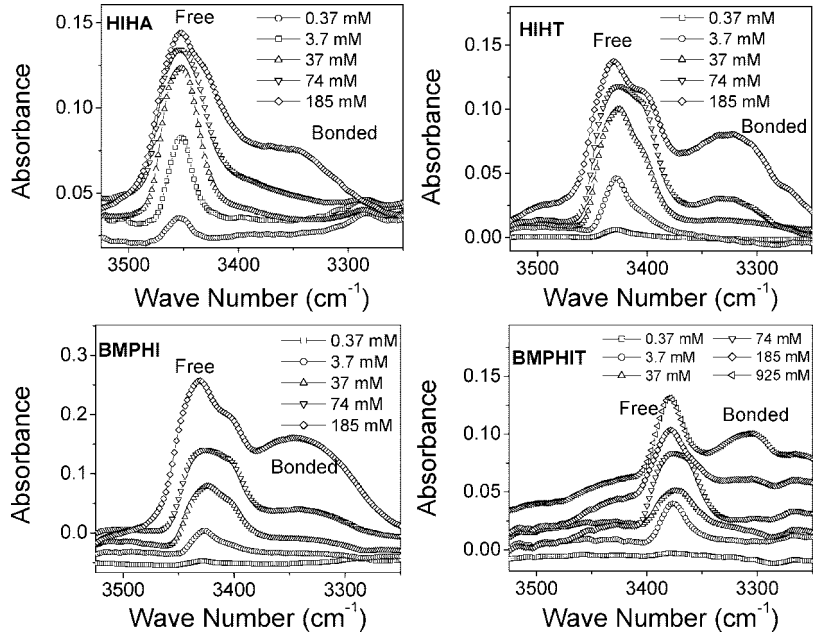

Figure 1. IR spectra of model compounds dissolved in chloroform. Note that the extra "bump" in the spectra for HIHA, HIHT, and BMPHI between 3400 and 3500 cm^{-1} is an instrumental artifact.

10 °C/min and a TA Q800 dynamic mechanical analysis (DMA) operating at 1 Hz and 3 °C/min. DMA was conducted in the tensile mode for 18 × 5 mm size samples with thickness of 120−200 μm. In DSC measurements, two heating scans were conducted for all samples, and the second scan were selected to determine T_g values using TA Universal Analysis software (V 3.9A). In DMA measurements, the temperature at the tan δ peak maximum was recorded as the T_g of the sample measured. Tensile properties measurements were conducted at room temperature on the TA Q800 DMA using the strain rate module operating at a strain rate of 10%/min. A typical sample has a dimension of 18 × 2 mm ($L \times W$) and thickness of 120−200 μm. Pencil hardness was measured according to ASTM D-3363. The Persoz pendulum hardness was measured according to ASTM D-4366 using a BYK-Gardner pendulum hardness tester with a square frame pendulum. At least six tests were performed for each film (different parts of the film) coated on a glass substrate, and the average value of the six was taken as the final result. Adhesion tests were conducted according to ASTM D 3359-02 on glass. All of the computations of hydrogen bonding energy were performed using density function theory. The function employed was the three-parameter B3 hybrid function of Becke[26] and the LYP correlation function of Lee, Yang, and Parr.[27] The basis sets used were the correlationally consistent basis sets cc-pVDZ[28] and cc-pVTZ[29] created by Dunning and co-workers. The cc-pVDZ basis set uses a double-ζ description for valence electrons, while the cc-pVTZ basis employs a triple-ζ description for valence electrons. Both basis sets use a single-ζ description for core electrons, and both have a consistent set of polarization functions. Refractive index was measured by a Bausch & Lomb ABBE-3 L refractometer at 24 °C at a wavelength of 589 nm. 1-Bromonaphthalene was applied between the sample film and the prism shield. The density of the polymers was measured using a density column constructed from toluene and carbon tetrachloride according to ASTM-D 1505.

Results and Discussion

Model Compounds: Solution. To ascertain the position of hydrogen bonded and free N−H peaks, model compounds in solution were measured by infrared spectroscopy as described in the Experimental Section. The FTIR spectra of the carbamate (HIHA), thiocarbamates (HIHT and BMPHI), and the dithiocarbamate (BMPHIT) are shown in Figure 1. At very low concentrations, e.g., 0.37 and 3.7 mM, where the model compounds are unable to associate through hydrogen bonding, only free N−H stretching peaks appear at 3453 cm^{-1} (HIHA), 3428 cm^{-1} (HIHT), 3428 cm^{-1} (BMPHI), and 3376 cm^{-1} (BMPHIT). Generally, intermolecular hydrogen bonding is not likely to occur at a concentration lower than 10 mM in a nonpolar solvent.[30] Apparently, the difference in free N−H peaks position is due to a variation in N−H bonding strength caused by the electronegativity difference of sulfur and oxygen atoms in the urethane, thiourethane, and dithiourethane groups. At higher concentrations, e.g., 74 and 185 mM, however, both the free N−H peak at higher frequencies and the hydrogen-bonded N−H peak at lower frequencies are present. A big difference is observed between the spectra of BMPHI and BMPHIT. A significant contribution from the NH hydrogen bonded to the carbonyl oxygen is present in the BMPHI solution at a concentration of 185 mM, while for the dithiocarbamate BMPHIT, the hydrogen bonded NH peak is only found at a much higher concentration, i.e., 925 mM. This indicates a lower propensity for hydrogen bonding for the dithiocarbamate in solution compared to the carbamate and thiocarbamate.

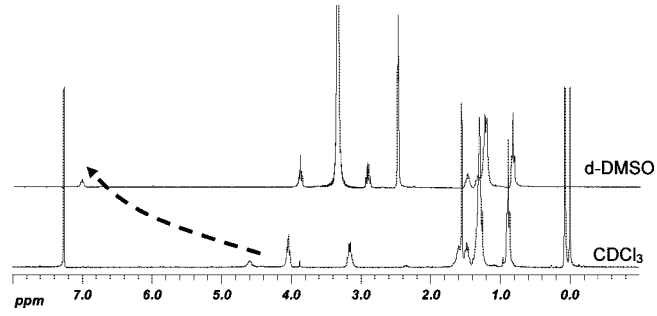

Figure 2. ^1H NMR spectra of 3.7 mM HIHA in $CDCl_3$ and d-DMSO.

To confirm the above observations, the model compounds were dissolved in both polar and nonpolar solvents and the ^1H NMR recorded to determine the effect of hydrogen bonding on the chemical shifts of the NH protons. Figure 2 shows the NMR spectra of HIHA in neat d-DMSO and $CDCl_3$ as an example. Recalling the results from Figure 1, it is noted that the concentration (3.7 mM) is so low that no intermolecular

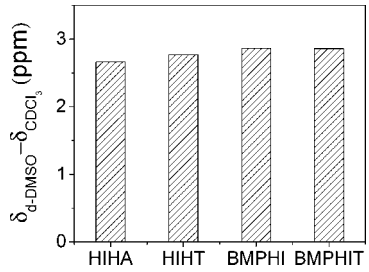

Figure 3. Chemical shift difference between NH protons in d-DMSO and $CDCl_3$.

hydrogen bonds are formed between HIHA molecules in the nonpolar solvent ($CDCl_3$) and by inference in d-DMSO. The only possible hydrogen bonding is between HIHA and d-DMSO. In d-DMSO, hydrogen bonds are formed between the model compound NH groups and the sulfinyl group (−S═O) of d-DMSO, resulting in a downfield shift of the NH proton peak due to a decrease in electron density around the NH proton and a corresponding increase in the asymmetry of the electron density due to the polarization of the NH bond by the −S═O group.[31] The extent of this shift, or the difference in chemical shifts for associated and unassociated NH, is a direct indication of the ability of the NH group to form hydrogen bonds with an oxygen acceptor.[31] The stronger the hydrogen bond formed, the greater the downfield shift. As already mentioned, the unassociated NH chemical shift refers to that at infinite dilution. This was confirmed since the NMR results show no significant change in the NH peak upon diluting the HIHA/$CDCl_3$ solution to as low as 0.37 mM (not shown). The chemical shift of the NH in $CDCl_3$ (3.7 mM) can thus be regarded as the unassociated value for comparison purposes. The chemical shift of NH in d-DMSO can then be taken as the associated NH value representing the hydrogen bonding between the NH of HIHA and the sulfinyl group of d-DMSO. NMR spectra were recorded for all the model compounds in a similar manner to that for HIHA in Figure 2, and the results are plotted in Figure 3. As shown in Figure 3, there is only a small difference in the values ($\delta_{d\text{-}DMSO} - \delta_{CDCl_3}$) obtained for HIHA and HIHT, indicating similar strengths of the carbamate and thiocarbamate hydrogen bonds. Also, BMPHIT does not show a lower shift value than BMPHI, indicating that the hydrogen bonding forming ability of the donor group, NH, is not adversely affected by the substitution of the carbonyl group with the thiocarbonyl. This suggests that the lower extent of hydrogen bonding found by FTIR in Figure 1 for BMPHIT results from the effect of the thiocarbamate on the hydrogen bonding capability.

Another interesting characteristic of BMPHI and BMPHIT is the intramolecular hydrogen bonding that forms between the NH proton and the ester carbonyl hydrogen bonding acceptor, in addition to the NH proton hydrogen bonding with the carbonyl on the carbamate/dithiocarbamate group. An effective way to quantify the extent of intramolecular hydrogen bonding can be expressed as

$$\mathrm{vr} = \frac{\delta_{d\text{-}DMSO} - \delta_{CDCl_3}}{\delta_{ref}} \qquad (1)$$

where δ_{ref} is the chemical shift of a reference compound with a similar structure to the compound being evaluated, but free of intramolecular hydrogen bonding.[32,33] A vr value smaller than 1.0 indicates the formation of intramolecular hydrogen bonding; the smaller the value, the greater the extent of intramolecular hydrogen bonding. Because of the similar structures of HIHT and BMPHI, HIHT can serve as a reference compound for BMPHI for comparison purposes. The calculated vr value of 1.03 indicates that no intramolecular hydrogen bonds are formed. If any such bonds were formed, a significant bonded IR peak should have also been observed at the concentrations around 3.7 mM.[34] As has already been shown in Figures 1 and 2, this is clearly not the case for either BMPHI or BMPHIT.

Table 1. Melting Point (T_m) of Small Model Compounds Measured by DSC Operating at 1 °C/min

	HIHA	HIHT	BMPHI	BMPHIT
T_m (°C)	10	24	31	5

Model Compounds: Melt. The melting points of the small model compounds measured by DSC are listed in Table 1. The two thiocarbamates have similar melting points, higher than those of the carbamate and the dithiocarbamate. The melting point is influenced by hydrogen bonding as well as other factors related to the unit crystal structure. Temperature-resolved infrared spectroscopy, an effective technique that has been extensively used to investigate hydrogen bonding,[6,7,31,35] was employed to measure the hydrogen bonding behavior of model compounds on a semiquantitative basis. Two distinctly separated NH peaks, representing free (higher frequency) and bonded (lower frequency) groups, are observed within the NH stretching region of HIHA and HIHT (Figure 4). A reduction in the bonded peak intensity and a corresponding increase in the intensity of the free peak with increasing temperature clearly illustrates disassociation of hydrogen bonds at elevated temperature. Similar changes are also observed in the IR spectra of BMPHI and BMPHIT. However, compared with the symmetrical and sharp bonded peaks of HIHA and HIHT, the bonded NH stretch bands of BMPHI and BMPHIT are unsymmetrical and much broader than those of HIHA and HIHT (Figure 4).

The absorbance of each peak, free and bonded, obtained through a peak deconvolution method described previously,[25] can be used to approximate the hydrogen bonding fraction ($F_{b,NH}$), the percent of NH groups involved in hydrogen bonding, based on the following equation[5,36]

$$F_{b,NH} = \frac{1}{1 + 3.46\dfrac{A_{f,NH}}{A_{b,NH}}} \qquad (2)$$

where $A_{f,NH}$ and $A_{b,NH}$ are the absorbance of free and hydrogen bonded NH groups, respectively, and the constant 3.46 is used as the extinction coefficient ratio of the bonded and free NH groups. Although, as stated in the literature,[4] the extinction coefficient of the NH group changes with the strength of the hydrogen bond, for semiquantitative comparison purposes, the error introduced by using 3.46 is minimal.

The NH stretching region of HIHA and HIHT can be deconvoluted into two distinct peaks, the free NH and the bonded NH peak. In the deconvolution process applied to BMPHI and BMPHIT, however, to obtain satisfactory curve fits, two peaks must be included in the bonded region (Figure 5). This is reasonable considering that two types of hydrogen bonding acceptors exist for BMPHI and BMPHIT: the ester carbonyl and the thiocarbamate carbonyl or dithiocarbamate thiocarbonyl. The competition between different types of acceptors are well-known in similar polyester and polyether urethanes.[5,37−39] The assignments of all the peaks are listed in Table 2 for comparison. The thiocarbamate bonded peaks in HIHT and BMPHI appear at exactly the same frequency with the same frequency shift value ($\Delta\nu$). The two NH-ester bonded peaks in BMPHI and BMPHIT appear at different frequencies as a result of differences in electron density, consistent with reported shifts of about 80 cm^{-1} for carbamate systems.[5,37] The hydrogen bonding fractions of each sample as a function of temperature, calculated using eq 2, are shown in Figure 6. It is

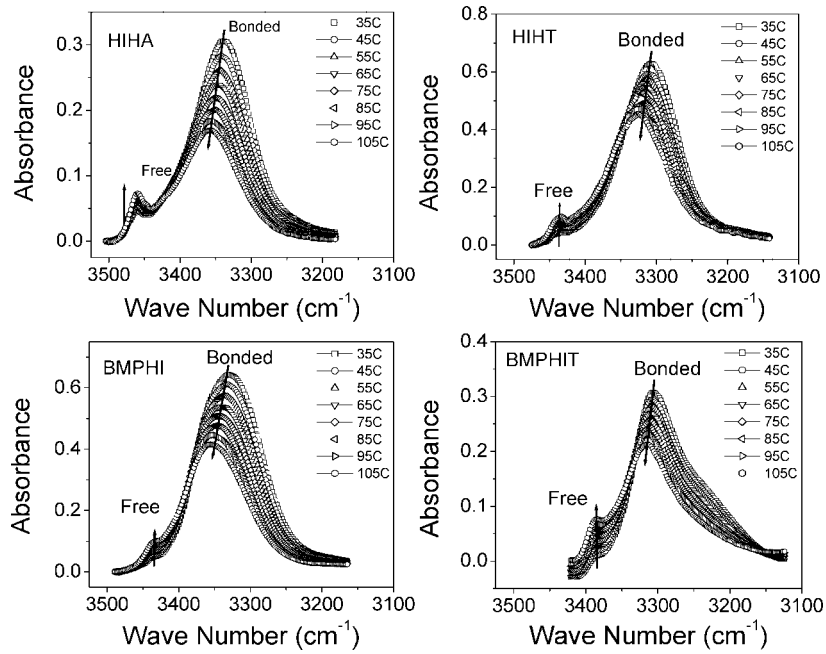

Figure 4. FTIR spectra of HIHA, HIHT, BMPHI, and BMPHIT measured at different temperatures. The arrows indicate the direction of peak intensity as a function of temperature increase.

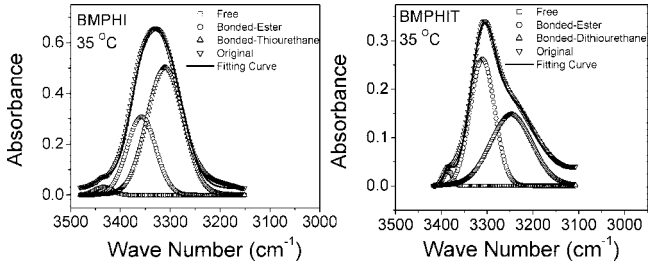

Figure 5. Peak deconvolution of the IR spectra of BMPHI and BMPHIT measured at 35 °C.

Table 2. Assignments of Free and Hydrogen Bonded Peaks in Model Compounds at 35 °C

	free	bonded peak (acceptor 1)		bonded peak (acceptor 2)	
	wavenumber (cm^{-1})	wavenumber (cm^{-1})	$\Delta\nu^a$ (cm^{-1})	wavenumber (cm^{-1})	$\Delta\nu$ (cm^{-1})
			urethane		
HIHA	3459	3340	119		
			thiourethane		
HIHT	3434	3311	123		
		thiourethane		ester	
BMPHI	3434	3311	123	3358	76
		dithiourethane		ester	
BMPHIT	3385	3247	138	3310	75

[a] $\Delta\nu$ is the wavenumber difference between bonded and free peaks.

noted that the $A_{b,NH}$ values used for BMPHI and BMPHIT in eq 2 are the result of adding the absorbances of the ester bonded peaks and the thiocarbamate/dithiocarbamate bonded peaks. In each case, with an increase in temperature, the hydrogen bonding fraction decreases as a result of disassociation. HIHA and HIHT show very similar hydrogen bonding fractions at a given temperature, indicative of similar hydrogen bonding ability. Because of the abundant hydrogen bonding acceptors present, BMPHI has the greatest extent of hydrogen bonding at a given temperature. Although the dithiocarbamate, BMPHIT, as a result of a high concentration of carbonyl acceptors, still has a hydrogen bonding fraction of over 70%, the lower hydrogen

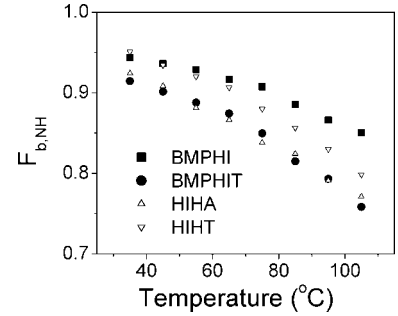

Figure 6. Hydrogen bonding fractions of model compounds.

bonding forming ability of the thiocarbonyl results in measurably lower hydrogen bonding fraction at a given temperature than its thiocarbamate analogue. These results are in agreement with the reported lower hydrogen bonding ability of the thiocarbonyl (C═S) group compared to the carbonyl group (C═O) determined by FTIR and crystallographic measurements.[22,40]

The contributions of ester, thiocarbamate, and dithiocarbamate groups can be quantitatively expressed by

$$C_{\text{ester}} = \frac{A_{\text{b,ester}}}{A_{\text{b,ester}} + A_{\text{b,thiocarbamate}}} \tag{3}$$

$$C_{\text{thiocarbamate}} = \frac{A_{\text{b,thiocarbamate}}}{A_{\text{b,ester}} + A_{\text{b,thiocarbamate}}} \tag{4}$$

$$C_{\text{dithiocarbamate}} = \frac{A_{\text{b,dithiocarbamate}}}{A_{\text{b,ester}} + A_{\text{b,dithiocarbamate}}} \tag{5}$$

where C and A stand for the contribution and the NH group absorbance, respectively. Although the extinction coefficient of NH groups bonded with different acceptors may be different, the results of these simple calculations are still reasonable for comparison purposes. As shown in Figure 7, for the thiocarbamate, BMPHI, the initial fractional contribution (35 °C) of the ester group, 0.33, is much lower than that of the thiocarbamate group, 0.67. These values change very little with an

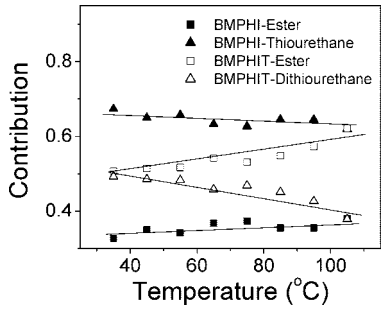

Figure 7. Contributions of different hydrogen bonding acceptors of BMPHI and BMPHIT model compounds.

increase in temperature. Interestingly, for BMPHIT, at room temperature, equal amounts of hydrogen bonds are formed between the NH hydrogen and the ester carbonyl and thiocarbonyl groups. With an increase in temperature, the fractional contribution of the ester groups sharply increases to over 0.6 while that of the dithiocarbamate groups decreases to less than 0.4. Model compounds were also investigated with temperature-resolved ^{1}H NMR spectroscopy. For all of the model compounds (the results for HIHA in Figure 8 are shown as an example), the NH peaks exhibit an upfield shift (Figure 9) due to the disassociation of hydrogen bonds as temperature increases, while the positions of all other peaks remain unchanged.

Theoretical Calculations. In order to substantiate the experimental results, ab initio calculations of hydrogen bonding energies were conducted for carbamate, thiocarbamate, and dithiocarbamate models. To simplify the calculation process, the model compounds shown in Chart 1 were used to conduct the theoretical calculation. The conclusions regarding the relative strength of hydrogen bondings can be readily extended to the more complicated models in Scheme 1. As shown in Table 3, the carbamate and the thiocarbamate models have almost identical hydrogen bonding energies between N−H and C═O, while weaker hydrogen bonds are calculated for the dithiocarbamate model. This supports the experimental FTIR and NMR results. We note that, on the basis of the theoretical hydrogen bonding energies in Table 3 and the margin of error in the theoretical calculations, it is not possible to predict whether the carbamate or the thiocarbamate has a higher hydrogen bonding energy.

Polymer Networks. To achieve an understanding of the hydrogen bonding behavior of carbamate, thiocarbamate, and dithiocarbamate groups when incorporated into polymer structures, a polyurethane, two polythiourethanes, and a polydithiourethane were prepared as described in the Experimental Section (see Scheme 2 for polymer acronyms). The mechanical, spectral, and thermal properties of the 3NCO-HexDiol and 3NCO-HexDithiol networks have been measured to provide an evaluation of any differences between the urethane (−N(H)−C(═O)−O−) and thiourethane (−N(H)−C(═O)−S−) linkages in the representative polymer networks. Differences in hydrogen bonding between thiourethane and dithiourethane (−N(H)−C(═S)−S−) groups in the networks will be evaluated by comparing corresponding experimental results for HDI-TriThiol and HDIT-TriThiol. Before continuing, we point out that the protocol used to cure each film resulted in essentially quantitative conversion (confirmed by FTIR) of all isocyanates and isothiocyanates in each case. However, in the case of the 3NCO-HexDiol films, although the curing takes place in a dry N_2 atmosphere, there is the potential for side reactions which may consume some of the isocyanate groups.[41]

Table 3. Hydrogen Bonding Energy of Carbamate, Thiocarbamate, and Dithiocarbamate

	carbamate	thiocarbamate	dithiocarbamate
hydrogen bonding energy (kcal/mol)	5.36	5.18	4.44

Table 4. Glass Transition Temperatures of Polymer Networks Measured by DSC and DMA

	3NCO-HexDiol	3NCO-HexDithiol	HDI-TriThiol	HDIT-TriThiol
DSC (°C)	48	50	45	35
DMA (°C)	69	67	65	55

Table 5. Pendulum Hardness and Pencil Hardness of Polymer Networks

	3NCO-HexDiol	3NCO-HexDithiol	HDI-TriThiol	HDIT-TriThiol
pendulum hardness (s)	266 ± 3.0	270 ± 6.9	287 ± 5.3	178 ± 5.5
pencil hardness	5H	5H	5H	H
cross hatch adhesion	5B	5B	5B	5B

Thermogravametric analysis of each polymer was first conducted (Figure 10) at a heating rate of 20 °C/min. For 3NCO-HexDiol and 3NCO-HexDithiol, the onset of weight loss of the urethane and thiourethane linkages occurred at 291 and 258 °C, respectively, followed presumably by decomposition of the isocyanurate at temperatures greater than 380 °C.[42] An enhanced thermal stability of the polyurethane is attributed to the higher bond energy of the C−O bond than the C−S bond.[43] HDI-TriThiol and HDIT-TriThiol also show a two-step decomposition process involving the thermal decomposition of the thiourethane and dithiourethane linkages followed by decomposition of the TriThiol segments at higher temperatures. The lower thermal stability of the polydithiourethane is consistent with a literature report that dithiourethanes undergo decomposition at temperatures between 150 and 200 °C with the aid of $AgNO_3$.[44] While the conditions for thermal decomposition in Figure 10 certainly do not involve a catalytic process, the low onset temperature is consistent with that reported by Gomez et al.[44]

Following the analysis used in the investigation of the small molecule models, temperature-resolved FTIR spectral measurements were also made for the four urethane-type polymers over a temperature range from 25 to 125 °C. Figure 11 shows a plot of the hydrogen bonding fraction of polymer networks as a

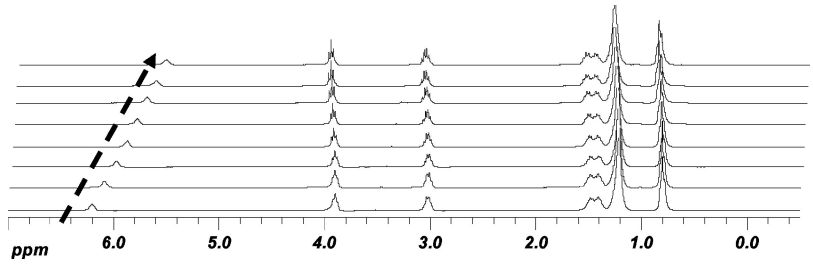

Figure 8. ^{1}H NMR spectra of HIHA (melt) measured at temperatures from 35 to 105 °C with a 10 °C interval. Small amount of d-DMSO was sealed in a capillary tube and inserted into the NMR tube for locking purpose.

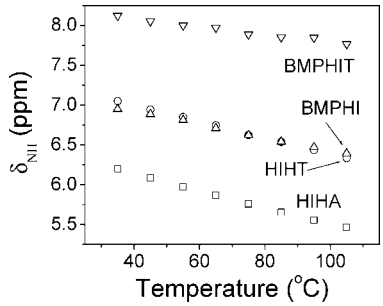

Figure 9. Chemical shift value of NH proton for model compounds as a function of temperature.

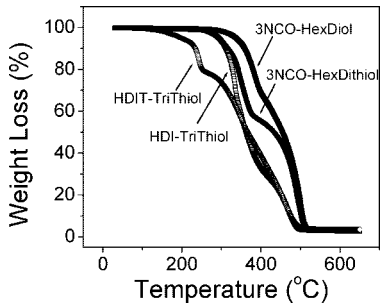

Figure 10. Thermogravimetric analysis of polymer networks.

Chart 1. Molecular Structures of (a) *N*-Methyl Methylcarbamate, (b) *N*-Methyl *S*-Methylthiocarbamate, and (c) *N*-Methyl *S*-Methyldithiocarbamate Used in Hydrogen Bonding Strength Calculation

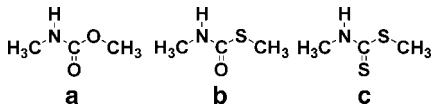

function of temperature that is consistent with the results for the small molecule models. At a given temperature, the fraction of hydrogen bonding for the polyurethane and two polythiourethane networks is greater than the hydrogen bonding fraction for the polydithiourethane. The thiourethane, HDI-TriThiol, benefits from the less sterically hindered ester groups of the flexible trithiol-based species, resulting in the highest extent of hydrogen bonding. As observed for the small molecule compounds, analysis of the contributions of the two different carbonyl donors in HDI-TriThiol and HDIT-TriThiol indicates that the thiourethane carbonyl dominates the hydrogen bonding in the former polymer, while the fractional contribution of the ester to the total hydrogen bonding is greater than for the thiocarbonyl groups in the polydithiourethane at a given temperature (Figure 12).

In an attempt to determine any physical/thermal differences in the four urethane type polymers, a battery of thermal and mechanical property measurements was made. The DSC thermal scans in Figure 13, and corresponding T_g values in Table 4, are all above room temperature, although the T_g for HDIT-Trithiol is not much greater than room temperature. The T_g of 3NCO-HexDithiol is only 2 °C greater than 3NCO-HexDiol. Its glass transition region is very narrow, and there is a distinct enthalpy relaxation peak. These results are strong indication of a very uniform structure in the case of the 3NCO-HexDithiol network. The polythiourethane (HDI-TriThiol) has a higher T_g than that of the polydithiourethane (HDIT-TriThiol). This can be attributed to the chain rigidity afforded by the higher hydrogen bonding fraction and hydrogen bond strength for HDI-Trithiol compared to HDIT-TriThiol (see Figures 11 and 12). However, it should be noted that the T_g difference between the polythiourethane and the polydithiourethane is only ~10 °C, and both have narrow glass transitions and enthalpy relaxation peaks as evidenced by the DSC scans in Figure 13. This is indicative of very uniform networks. The narrow glass transition regions found in the DSC scans in Figure 13 are confirmed by the DMA plots in Figure 14 for the 3NCO-HexDithiol and the HDI-TriThiol networks which have full width at half-maximum (fwhm) temperature ranges of 14 and 12 °C, respectively, considerably smaller than the fwhm values for their 3NCO-HexDiol (30 °C) and HDIT-TriThiol (20 °C) counterparts. The very low fwhm values for HDI-TriThiol and 3NCO-HexDithiol are suggestive of and consistent with very efficient reactions between the aliphatic isocyanates and thiols with little or no side products, e.g., allophanate, compared to the isocyanate−alcohol reactions used to make the 3NCO-HexDiol network, which are well documented[45] to undergo side reactions presumably resulting in broadening of the thermal (Figure 13) and mechanical (Figure 14) transitions. The near quantitative conversions for the reactions of isocyanates and thiols with no side products are indeed well documented.[19,24,46] Interestingly, the HDIT-TriThiol network formed by reactions between the isothiocyanate and thiols also have very narrow glass transition regions, although the T_g of the HDIT-TriThiol network is lower than that of the HDI-TriThiol network due presumably to the higher extent of hydrogen bonding (and lower T_g) for the latter. Returning again to the results in Figures 13 and 14, we reiterate that it is remarkable that such narrow transitions occur in such

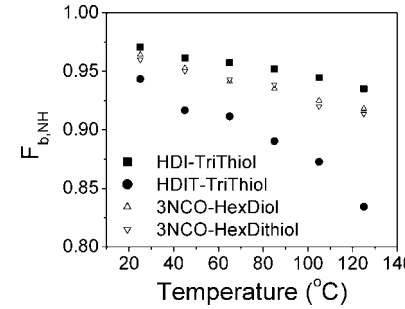

Figure 11. Hydrogen bonding fraction of polymer networks as a function of temperature.

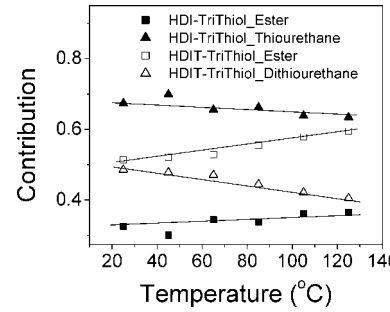

Figure 12. Contributions of different hydrogen bonding acceptors of HDI-TriThiol and HDIT-TriThiol.

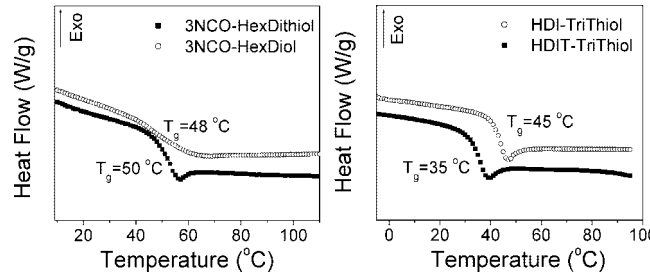

Figure 13. DSC scans of polymer networks.

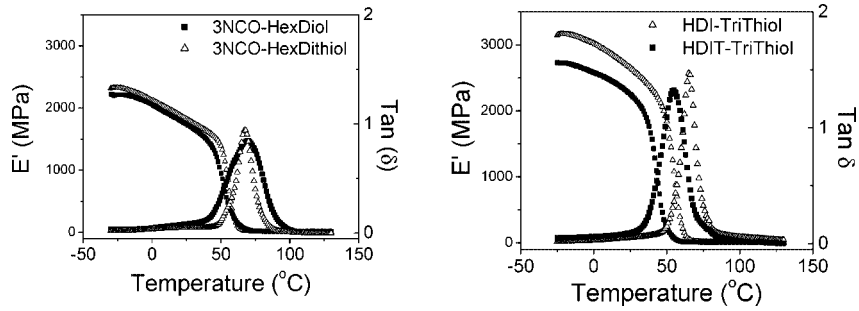

Figure 14. Storage modulus (E') and tan δ of polymer networks measured by DMA operating at 3 °C/min.

Table 6. Yield Stress (σ_y), Yield Strain (ε_y), Stress at Break (σ_b), Strain at Break (ε_b), and Young's Modulus (E) of Polymer Networks

	σ_y (MPa)	ε_y (%)	σ_b (MPa)	ε_b (%)	E (MPa)
3NCO-HexDiol	19.99 ± 2.68	3.48 ± 0.56	33.41 ± 3.26	91.73 ± 3.92	1057.83 ± 98.37
3NCO-HexDithiol	19.94 ± 0.63	3.73 ± 0.80	28.62 ± 0.60	90.52 ± 1.73	1074.68 ± 69.77
HDI-TriThiol	30.71 ± 3.44	3.97 ± 2.19	32.13 ± 3.05	107.80 ± 5.40	1676.60 ± 77.90
HDIT-TriThiol	4.67 ± 1.11	4.77 ± 1.50	27.83 ± 5.01	125.00 ± 6.88	310.50 ± 34.76

Table 7. Densities and Refractive Indices of Polymer Networks

	3NCO-HexDiol	3NCO-HexDithiol	HDI-TriThiol	HDIT-TriThiol
density (g/cm^3)	1.2518	1.2466	1.2698	1.2795
refractive index	1.5151	1.5505	1.5470	1.6092

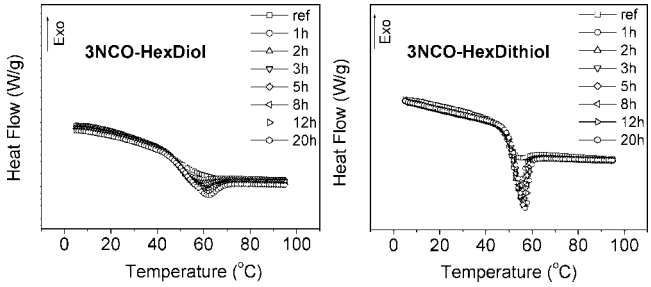

Figure 15. DSC curves of 3NCO-HexDiol and 3NCO-HexDithiol networks annealed for different times.

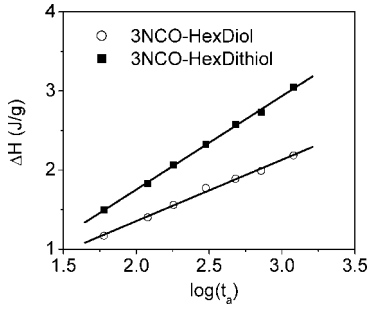

Figure 16. Enthalpy relaxation of 3NCO-HexDiol and 3NCO-HexDithiol as a function of sub-T_g aging time.

high-density networks. These results are reminiscent of the results obtained by photoinitiated thiol−ene free-radical step-growth polymerization where highly uniform networks are also formed.[23,47,48] The thiol−isocyanate reaction is a clear candidate for a "click" process characterized by essentially quantitative conversions obtained under relatively benign conditions with little or no side reactions.[49] This premise is under evaluation and will be reported on in future publications.

Although 3NCO-HexDiol and 3NCO-HexDithiol have many similar properties as have been and will be shown, they still have some differences resulting from the network structure as discussed previously. To follow up on these differences, sub-T_g aging studies were conducted. DSC heating scans obtained after annealing, i.e., physical aging, at T_g-10 °C for 3NCO-HexDiol and 3NCO-HexDithiol for a specific period of time are shown in Figure 15. As is well-known for many linear polymers,[50] and is demonstrated in Figure 15 for the urethane and thiourethane polymer networks, the enthalpy relaxation peak increases with the annealing time. The relaxed enthalpy, obtained from the integration of the enthalpy relaxation peak, and relaxation rate are different for the two networks as is obvious from the plots of the relaxed enthalpy versus time in Figure 16. The faster rate of enthalpy relaxation for 3NCO-HexDithiol compared to 3NCO-HexDiol is consistent with the narrowness of the glass transition region.

3NCO-HexDiol, 3NCO-HexDithiol, and HDI-TriThiol all exhibit similar pendulum hardness, indicating that energy damping even at 25 °C, well below the T_g of each polymer, is similar for all three systems (Table 5). The polydithiourethane (HDIT-TriThiol), however, exhibits significantly greater damping; i.e., the oscillation time is about 100 s lower than for the other three polymer films. This no doubt reflects the lower hydrogen bonding (and lower T_g) for HDIT-TriThiol and corresponding greater energy dissipation (i.e., energy damping) at room temperature. The polyurethane and polythiourethanes also exhibit better surface scratch resistance as indicated by higher pencil hardness (Table 5), while all four of the urethane type polymers exhibited excellent adhesion to glass (Table 5). A number of factors, including mechanical interlocking, dipole−dipole interactions, and covalent bonding,[51] affect adhesion, and hence it is not surprising that all four polymers adhere well to glass.

Results obtained from stress−strain curves (Figure 17) of each system are listed in Table 6 for comparison. The stress−strain curves for 3NCO-HexDiol and the two polythiourethanes

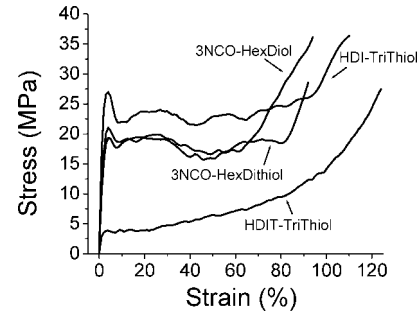

Figure 17. Representative stress−strain curves of model compounds measured at a strain rate of 10%/min.

(3NCO-HexDithiol and HDI-TriThiol) are typical of noncrystalline polymers. In the first region, tensile stress increases linearly with strain that is recoverable (obeying Hook's law) when the external force is removed, due to relaxation of bond length and bond angle, until the polymer yields. The larger hydrogen bond fraction no doubt plays a key role in explaining the higher yield stress of HDI-TriThiol compared to HDIT-TriThiol (Table 6). The comparable yield stress for 3NCO-HexDiol and 3NCO-HexDithiol is consistent with the near equivalency of hydrogen bonding. In the second region, a plateau is achieved after passing the yield point as a result of chain segmental motion. Tensile strains greater than 50% are achieved by a combination of stretching/orientation and coincident breaking of intermolecular interactions (i.e., van der Waals force and hydrogen bonding). Interestingly, the stress plateau for HDI-TriThiol, which has a higher fraction of hydrogen bonding according to the FTIR results in Figure 11, appears at a higher level than its polydithiourethane analogue. The polymers prepared from 3NCO have very similar tensile properties in the second region due to only minor differences in their structures and hydrogen bonding behavior. The tensile stress increases sharply in the third region for each urethane type polymer due to further stretching of the orientated structures. The final break is a result of covalent bonding cleavage and complete disassociation of secondary interactions such as van der Waals and hydrogen bonding. The difference between the stress at break (σ_b) of the two polymers prepared from 3NCO may well be due to the difference in bonding energy of C−O and C−S[43] since hydrogen bonding is almost equivalent for these two systems. The polydithiourethane exhibits the characteristics of rubbery materials, the tensile stress of which increases continuously after the linear elastic region until the polymer breaks at a relatively higher strain. This rubbery property and the lower tensile strength are partly the result of a lower fraction of hydrogen bonding, resulting in a relatively lower glass transition region near 25 °C. Summarizing, comparing HDI-TriThiol with the other three polymer networks, it is reasonable to conclude that a combination of appropriate flexibility in the backbone and abundant sterically accessible hydrogen bonding acceptor sites leads to a tough and hard urethane type material as indicated by Young's modulus, the energy to break (area below the stress−strain curve), and hardness.

Although comprehensive analysis and discussions on hydrogen bonding behavior of urethane type polymers have been made based on several types of measurements, there is still one critical parameter that needs to be evaluated. Since mechanical and optical properties of network films can be related to density, the densities of each system were measured (Table 7). The results show that all of the cured networks have approximately equivalent densities.

Finally, it is noted that a major interest in polythiourethane and polydithiourethanes is a result of their high refractive indices. The results in Table 7 clearly show that indeed the refractive index is directly related to the sulfur content in the films with 3NCO-HexDithiol having a higher refractive index than 3NCO-HexDiol and HDIT-TriThiol having the highest refractive index of all four systems.

Conclusions

A series of small molecule and polymeric urethane, thiourethane, and dithiourethane compounds were prepared and measured by FTIR, NMR, DSC, and DMA, establishing the order of the hydrogen bonding strength as carbamate ≈ thiocarbamate > dithiocarbamate. Because of their similar hydrogen bonding behavior, polyurethane and polythiourethane networks have similar physical and mechanical properties, i.e., T_g, hardness, and tensile properties. The polydithiourethane with lower T_g is softer, more flexible, and less tough because of weaker hydrogen bonding forming ability. The comprehensive characterization and comparison of urethane, thiourethane, and dithiourethane compounds reported herein provide experimental and theoretical guidance for various applications of sulfur-containing polyurethanes.

Acknowledgment. This work was supported by the MRSEC Program of the National Science Foundation under Award DMR 0213883. We also acknowledge Bayer Materials Science for supplying isocyanates and Bruno Bock Thiochemical for providing thiols.

References and Notes

(1) Bayer, O. *Angew. Chem.* **1947**, *A59*, 257.
(2) Chattopadhyay, D. K.; Raju, K. V. S. N. *Prog. Polym. Sci.* **2007**, *32*, 352.
(3) Pztrov, Z. S.; Ferguson, J. *Prog. Polym. Sci.* **1991**, *16*, 695.
(4) Coleman, M. M.; Lee, K. H.; Skrovanek, D. J.; Painter, P. C. *Macromolecules* **1986**, *19*, 2149–2157.
(5) Seymour, R. W.; Estes, G. M.; Cooper, S. L. *Macromolecules* **1970**, *3*, 579.
(6) Lee, H. S.; Wang, Y. K.; Hsu, S. L. *Macromolecules* **1987**, *20*, 2089.
(7) Pollack, S. K.; Smyth, G.; Papadimitrakopoulos, F.; Stenhouse, P. J.; Hsu, S. L.; MacKnight, W. J. *Macromolecules* **1992**, *25*, 2381–2390.
(8) Christenson, C. P.; Harthcock, M. A.; Meadows, M. D.; Spell, H. L.; Howard, W. L.; Creswick, M. W.; et al. *J. Polym. Sci., Part B: Polym. Phys.* **1986**, *24*, 1404.
(9) Mishra, A. K.; Chattopadhyay, D. K.; B, S.; Raju, K. V. S. N. *Prog. Org. Coat.* **2006**, *55*, 231.
(10) Wang, C. B.; Cooper, S. L. *Macromolecules* **1983**, *16*, 775.
(11) Yen, F.-S.; Hong, J.-L. *Macromolecules* **1997**, *30*, 7927.
(12) Dyer, E.; Osborne, D. W. *J. Polym. Sci.* **1960**, *47*, 361.
(13) Hastings, G. W.; Johnston, D. *Br. Polym. J.* **1971**, *3*, 83.
(14) Zhu, Z.; Risch, B. G.; Yang, Z.; Lin, Y.-N. European Patent Application EP0780413A1, **1997**.
(15) Zhou, Y.; Lin, Y.-N.; Zhu, Z.; Risch, B. G. US Patent US 6008296, **1999**.
(16) Tanaka, M.; et al. U.S. Patent Application 20050131203, **2005**.
(17) Shinohara, N.; et al. PCT International Application WO 2004078855, **2004**.
(18) Dietliker, K.; Misteli, K.; Jung, T.; Studer, K. In *RadTech Europe 05: UV/EB−Join the Winning Technology (Conference Proceedings), Barcelona, Spain, Oct. 18−20, 2005*; Barcelona, Spain, 2005; p 473.
(19) Dyer, E.; Glenn, J. F.; Lendrat, E. G. *J. Org. Chem.* **1961**, *26*, 2919.
(20) Freed, V. H.; et al. *J. Agric. Food Chem.* **1967**, *15*, 1121.
(21) Nagai, A.; Ochiiai, B.; Endo, T. *J. Polym. Sci., Part A: Polym. Chem.* **2005**, *43*, 1554.
(22) Wheeler, K. A.; Harrington, B.; Zapp, M.; Casey, E. *CrystEngComm* **2003**, *5*, 337.
(23) Li, Q.; Zhou, H.; Wicks, D. A.; Hoyle, C. E. *J. Polym. Sci., Part A: Polym. Chem.* **2007**, *45*, 5103–5111.
(24) Dyer, E.; Glenn, J. F. *J. Am. Chem. Soc.* **1957**, *79*, 366.
(25) Zhou, H.; Li, Q.; Lee, T. Y.; Guymon, A. C.; Jonsson, S. E.; Hoyle, C. E. *Macromolecules* **2006**, *39*, 8269–8273.
(26) Becke, A. D. *J. Chem. Phys.* **1993**, *98*, 5648.
(27) Lee, C.; Yang, W.; Parr, R. G. *Phys. Rev. B* **1988**, *37*, 785.
(28) Woon, D. E.; Dunning, T. H. *J. Chem. Phys.* **1993**, *98*, 1358.
(29) Kendall, R. A.; Dunning, T. H.; Harrison, R. J. *J. Chem. Phys.* **1992**, *96*, 6796.
(30) Silverstein, R. M.; Bassler, G. C.; Morrill, T. C. *Spectrometric Identification of Organic Compounds*, 4th ed.; John Wiley & Sons: New York, 1981.
(31) Joesten, M. D.; Schaad, L. J. *Hydrogen Bonding*; Marcel Dekker: New York, 1974.
(32) Barisic, L.; Cakic, M.; Mahmoud, K. A.; Liu, Y.-N.; Kraatz, H.-B.; Pritzkow, H.; Kirin, S. I.; Metzler-Nolte, M.; Rapic, V. *Chem.−Eur. J.* **2006**, *12*, 4965.
(33) Ishimoto, B.; Tonan, K.; Ikawa, S.-i. *Spectrochim. Acta, Part A* **1999**, *56*, 201.
(34) Winningham, M. J.; Sogah, D. Y. *J. Am. Chem. Soc.* **1994**, *116*, 11173.
(35) He, Y.; Zhu, B.; Inoue, Y. *Prog. Polym. Sci.* **2004**, *29*, 1021.
(36) Xiu, Y.; Zhang, Z.; Wang, D.; Ying, S.; Li, J. *Polymer* **1992**, *33*, 1335.
(37) Boyarchuk, Y. M.; Rappoport, L. Y.; Nikitin, V. N.; Apukhtine, N. P. *Polym. Sci. USSR* **1965**, *7*, 859.
(38) Tanaka, T.; Yokoyama, T.; Yamuguchi, Y. *J. Polym. Sci., Part A-1* **1968**, *6*, 2137.
(39) Nakayama, K.; Ino, T.; Matsubara, I. *J. Macromol. Sci., Chem.* **1969**, *A3*, 1005.

(40) Gramstad, T.; Sandstrom, H. J. *Spectrochim. Acta* **1969**, *25A*, 31.
(41) Oertel, G. *Polyurethane Handbook*, 2nd ed.; Hanser Publishers: Munich, 1993.
(42) Kordomenos, P. I.; Kresta, J. E.; Frisch, K. C. *Macromolecules* **1987**, *20*, 2077.
(43) Douglas, B.; McDaniel, D.; Alexander, J. *Concepts and Models of Inorganic Chemistry*, 3rd ed.; John Wiley & Sons: New York, 1994.
(44) Gomez, L.; Gellibert, F.; Wagner, A.; Mioskowski, C. *J. Comb. Chem.* **2000**, *2*, 75.
(45) Frisch, K. C.; Rumao, L. P. *J. Macromol. Sci., Rev. Macromol. Chem.* **1970**, *C5*, 103.
(46) Klemm, E.; Stockl, C. *Makromol. Chem.* **1991**, *192*, 153.
(47) Hoyle, C. E.; Lee, T. Y.; Roper, T. *J. Polym. Sci., Part A: Polym. Chem.* **2004**, *42*, 5301.
(48) Wei, H.; Li, Q.; Ojelade, M.; Madbouly, S.; Otaigbe, J. U.; Hoyle, C. E. *Macromolecules* **2007**, *40*, 8788.
(49) Kolb, H. C.; Finn, M. G.; Sharpless, K. B. *Angew. Chem., Int. Ed.* **2001**, *40*, 2004.
(50) Hutchinson, J. M. *Prog. Polym. Sci.* **1995**, *20*, 703–760.
(51) Woods, J. G. In *Radiation Curing: Science and Technology*; Pappas, S. P., Ed.; Springer: Berlin, 1992; p 333.

MA802848T